Airbursts and Cratering Impacts

2024 | Volume 2 | Pages: 1–23 | e-location ID: e20240002
DOI: 10.14293/ACI.2024.0002

Research Article

Kaş Bay: Evidence of a 20 km-diameter complex impact structure on the Turkey-Greece frontier

A.J. Ure[1,*], D.R. Bridgland[2], N. Tunstall[2], R. Westaway[3], S. Çakmak[4] and T. Demir[4]

[1]School of Environmental, Earth and Ecosystem Science, The Open University, Milton Keynes, UK; [2]Department of Geography, Durham University, Durham, UK; [3]Department of Earth Sciences, Glasgow University, Glasgow, UK; [4]Department of Geography Akdeniz University, Antalya, Turkey

*Correspondence to: A.J. Ure, E-mail: alijoure@hotmail.com

Received: 5 March 2024; Revised: 25 March 2024; Accepted: 5 April 2024; Published online: 29 April 2024

How to cite: Ure A.J., et al. Kaş Bay: Evidence of a 20 km-diameter complex impact structure on the Turkey-Greece frontier. *Airbursts and Cratering Impacts*. 2024 | Volume 2 | Issue 1 | Pages: 1–23 | DOI: 10.14293/ACI.2024.0002

ABSTRACT

Extensive field work, mineralogical and petrographic investigations show strong evidence for a complex, hypervelocity impact structure protruding into the Mediterranean Sea at the Turkey-Greece border. The Kaş Bay structure with a diameter of around 20 km, is structurally altered, since it coincides with the triple point of the Anatolian, Aegean, and African plates. The target rocks, entirely comprising sedimentary carbonate, show evidence of shock metamorphism, along with a wealth of significant finds and numerous indications of a clear and strong impact overprint. A Pleistocene age is inferred from related stratigraphical evidence.

KEYWORDS

mediterranean, digital terrain model, transtension/transpression, pleistocene, shock metamorphism

Introduction

Kaş is a small town on the Mediterranean coast of Southern Turkey located 36.1999° N, and 29.6396° E. The location is on the southern edge of the Teke Peninsula, roughly midway between Fethiye and Antalya, where the Greek Island of Kastellorizo separates Kaş Bay from the open sea (Figure 1). The adjacent Turkish coastline forms a semicircular arc, with multiple, roughly concentric, curved, linear hills.

The local bedrock is Cretaceous marine limestone, and because no local volcanism is evident, this potential geological origin of the circular structures can be excluded. An impact hypothesis was first suggested in 2016 after field investigations to ascertain the cause of the unusual geological features were undertaken. A small circular group of islands (Figure 2) in the SE part of Kaş Bay outlines an inverse cone-shaped area of shallow bathymetry. The top of this cone is ~1 km in diameter, with a gentle dish profile down to 20 m depth in its centre. Around the outer margins of these islands, delineating the top of the cone, is a near-vertical drop to 85 m depth. This remarkable circular structure has been proposed as the central uplift of a complex hypervelocity impact structure [1].

The reason that the Kaş Bay structure, despite its size, has not so far been recognized as an impact site is mainly

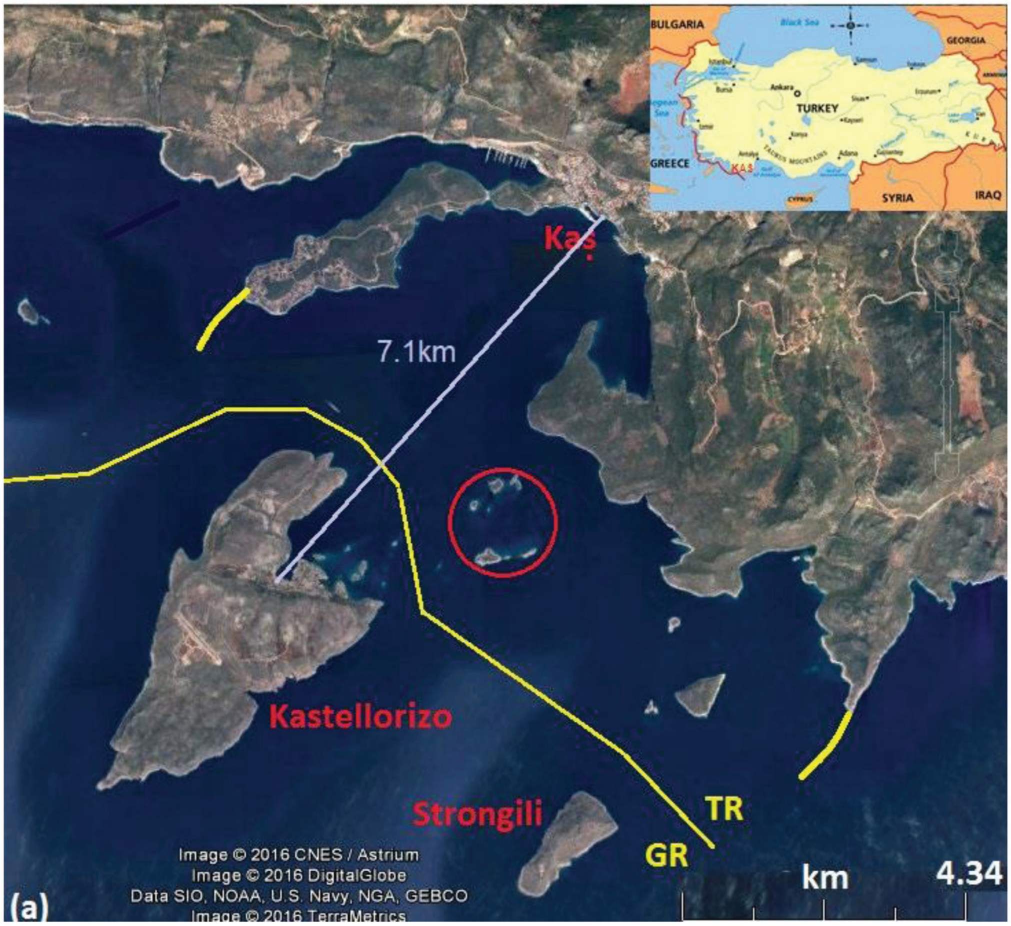

Figure 1: Google map image of Kaş Bay 2016, indicating the initial suggested crater rim, yellow curved lines. The unbroken yellow line demarcates the border between Greece and Turkey. Red circle shows the islands marking the central uplift.

Figure 2: View; the circular group of islands in Kaş Bay, looking southward with Strongili island in the background. Photo courtesy of David Talbot.

because its northeastern margin, in its continuation onto the Turkish landmass, no longer bears any resemblance to a round impact crater and is more elongated in configuration, and its southern and western margins have disappeared. This shape is indicated in Figures 3 and 4.

We explain this shape as being due to the location of Kaş in the subduction zone of the African and Eurasian plates near the boundary of the smaller associated Anatolian and Aegean plates, which move in different directions and at different speeds (Figure 3). After the impact, proposed to have occurred in the Pleistocene epoch [2], this plate movement caused the original, presumably round crater, to be disrupted and deformed, even possibly made smaller. Consequently, transpressional ridges and transtensional troughs [3] from the modification stage of the cratering process, can still be observed on land in the Digital Terrain Model (Figure 4), and on the adjacent sea floor of the receding Aegean plate (Figure 3).

The Western Taurus Mountains, including the Kaş region, with their notably rugged terrain, run parallel to the Mediterranean Sea in southern Turkey as an extension of the Alpine orogenic belt, forming a primary geomorphological component of the region. This mountain range extends along the islands of Crete and Rhodes, from the Teke Peninsula to Uzunyayla and the Elbistan Plain in the east, for more than 900 kilometres. The study area is located in the southern (coastal) section of the Western Taurus Mountains, stretching in an arc across the Teke Plateau to the Taşeli Plateau. Akdağ mountain is located north of the area, while the Bey Mountains and the Tahtalı Mountains are situated to the northeast. These mountain ranges, which include the region's highest summits (3070 m), are incised by deep canyons. Unlike the Central and Eastern Taurus Mountains, which continue in an east-west direction, the Western Taurus Mountains make a sharp bend along the line between Eğirdir Lake and Antalya Bay (Antalya Suture Belt) in a northeast-southwest direction.

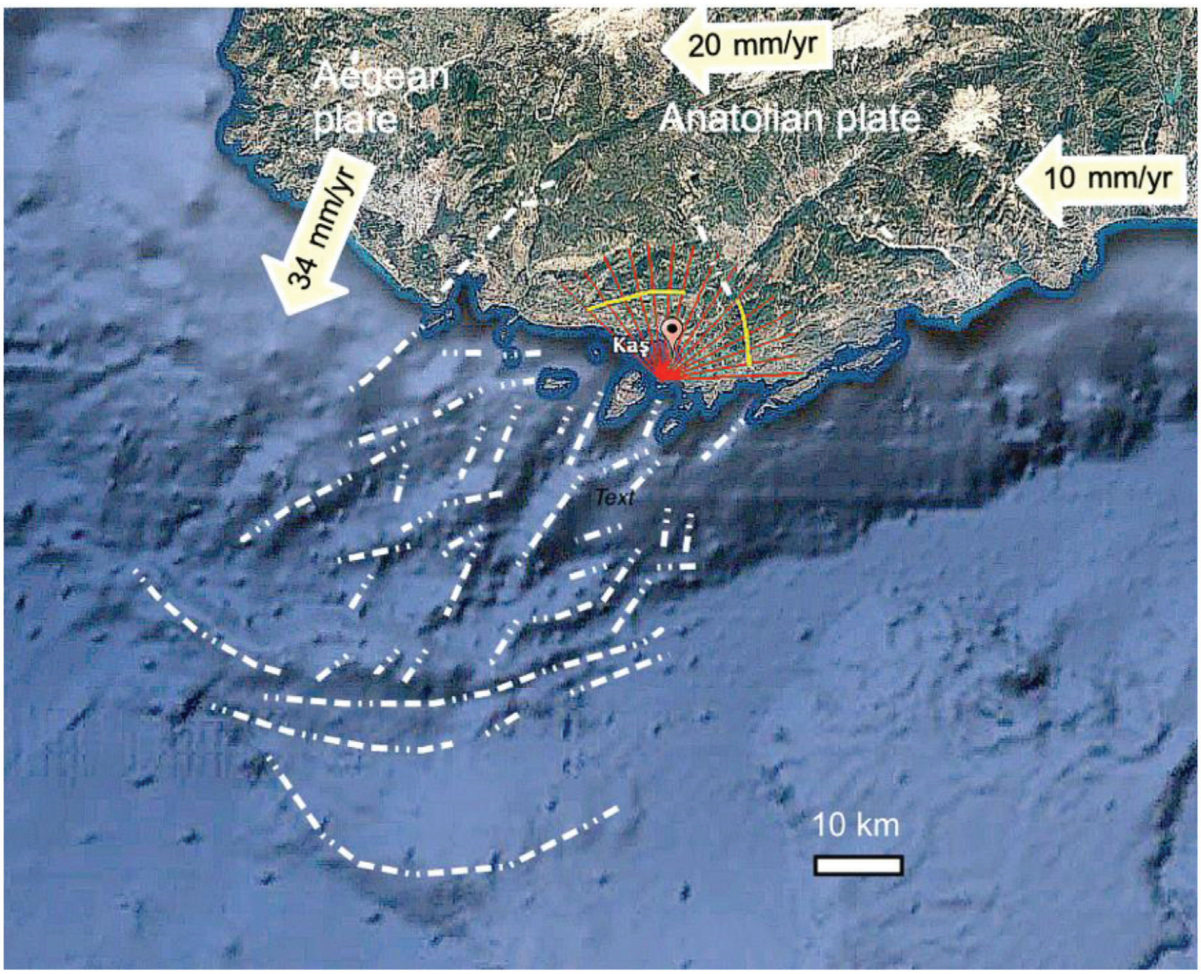

Figure 3: The radial sea floor structures are suggested to be remnants of the southern part of the original Kaş circular crater, with distortion and displacement resulting from movement of the Aegean plate relative to the Anatolian plate. The African plate moves northwest at around 2.15 cm per year [4].

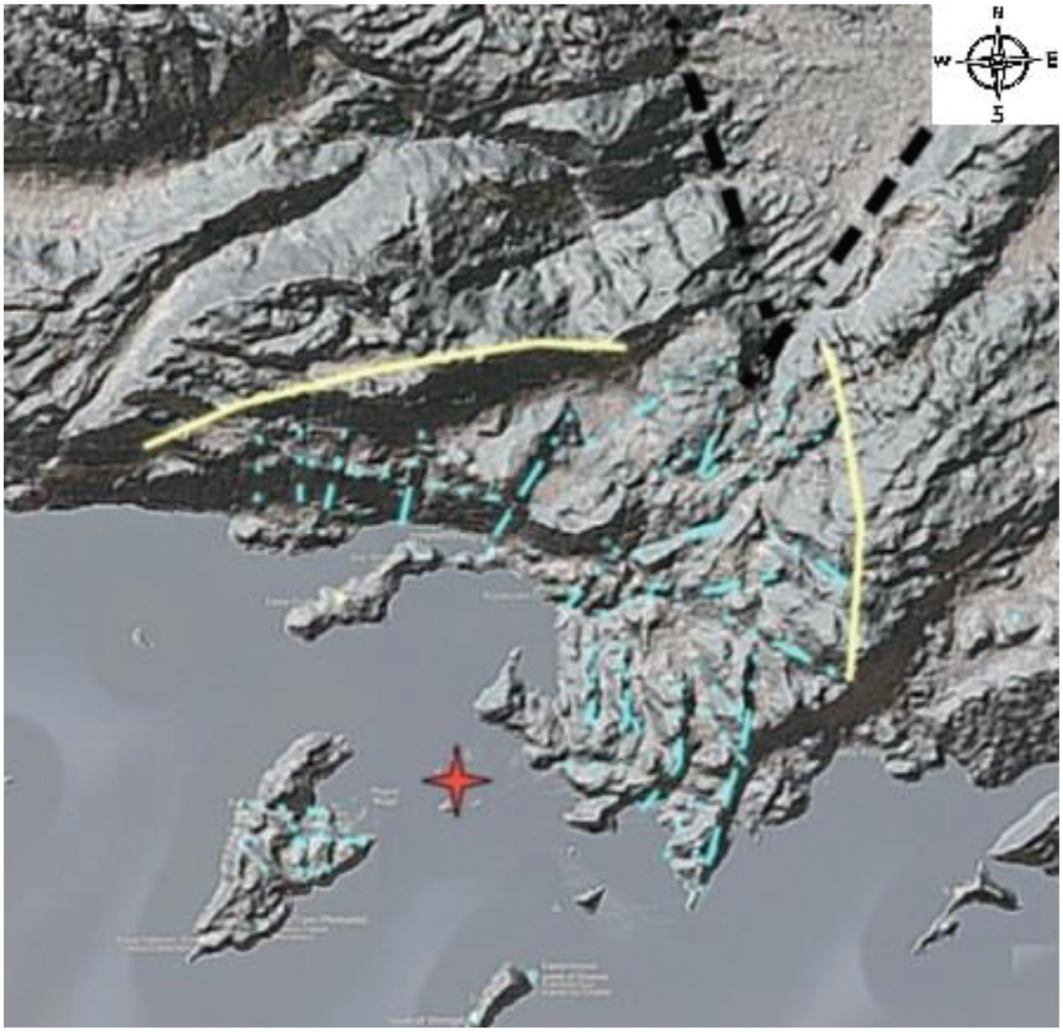

Figure 4: Digital Terrain Model images of the Kaş Bay impact structure onshore, mostly composed of an accumulation of smaller and bigger megablocks, some larger ones marked turquoise. The turquoise lines also represent probable transtensional troughs. Yellow lines indicate the proposed distorted crater rim.

Clayey and carbonate limestones deposited in the Tethys seas throughout the Mesozoic make up the lithological structure of the Western Taurus Mountains (Figure 5).

Geological-petrographic-mineralogical features, providing evidence for an impact, are widespread although, due to the lack of silicate rocks, shock metamorphism is restricted to carbonate rocks. In this case we suggest reconsidering the 'law of proven impact' commonly maintained within the impact community and giving substantially more credit to intrinsic geological evidence, especially when silicate rocks are lacking.

Method

Since 2016, extensive field studies have been conducted on mainland Turkey, on islands in Kaş Bay, and the island of Kastellorizo. These have included mapping and looking for impact-event characteristics, such as impact-related rock deformation, impact ejecta, shatter-cones, shock metamorphism, and signs of possible melt and decarbonization [6]. Samples were collected for various analyses that included thin-section preparation, XRF and magnetic susceptibility. In addition, a comparison was made with the Spanish Rubielos de la Cérida impact structure.

Early research suggested that the Kaş Bay Impact structure was 8–10 km in diameter [7]. The distance between Kastellorizo and Kaş town is 7.1 km [8] (Figure 1). The procurement of Digital Terrain Modelling (DTM) in December 2022 from satellite data over the site [9] indicated a structure much larger than this original suggestion, possibly ~20 km in diameter. This and further observations of the study area formed the basis of the latest field research executed in early 2023. In Figure 4, the yellow

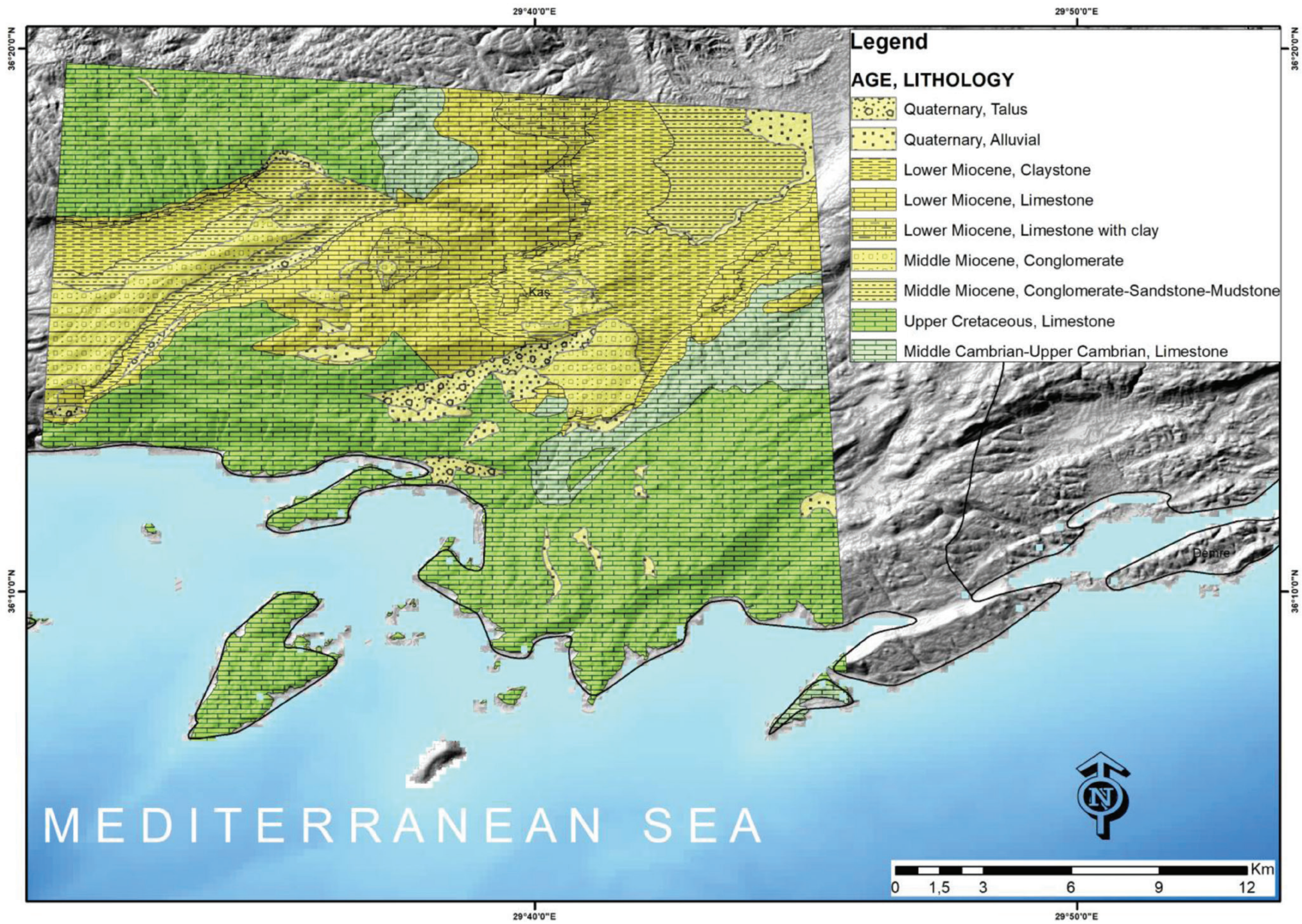

Figure 5: Geology of the Kaş area [5].

lines indicate the suggested new, albeit distorted, crater rim. Visual ground observations were undertaken to ascertain whether the field evidence supported this suggestion from the satellite imagery. The terrain is extremely scrubby and very steep (nearly vertical in places), but road cuttings and new building sites, along with old quarries, allowed visualisation of the geology.

A study of the geomorphology emphasized that the ground north of the Kaş peninsula has subsided. Turkey is highly active tectonically, and the proposed crater, along with the three aforementioned plates jostling for room, is no exception (Figure 3). A comparison of how different aspects of the geomorphology might reflect tectonic movement or an impact event was considered.

Results

Breccias

Breccias are a significant constituent of impact structures due to the established contact/compression, excavation, and modification stages of impact cratering [1]. The Kaş Bay structure is no exception, and the richness of both monomict and polymict breccias in the field, along with megabreccias and dyke breccias, is striking (Figures 6-9). Breccia dykes are a prominent feature in impact structures [10].

Breccia-in-breccia and Breccia Generations

Due to the various stages of impact cratering, breccias-within-breccias and, in particular, multiple breccia generations (Figures 10, 11), are a typical impact texture and rarely observed in other brecciation processes [11]. This unusual impact phenomenon is abundant throughout the study area.

Peculiar breccias, often referred to as fitted fragments [11] and containing coherent fractured clasts with preserved fitting (Figure 12), indicate movement under confining pressure conditions.

All the above impact-specific field evidence is abundant on mainland Turkey, the islands of the central uplift and Kastellorizo.

Spallation

In fracture mechanics, the spallation in solids (not to be confused with nuclear spallation) is well understood.

Figure 6: Monomict breccias – single clast breccia- including a Lycian tomb cut into monomict breccia.

Figure 7: Polymict breccias – multi clast breccia- including a polymict breccia quern.

Figure 8: Megabreccia – mega relates to breccia volume and clast size.

Figure 9: Breccia dykes of varying scales from above and below water, including in the rock-cut Lycian tomb.

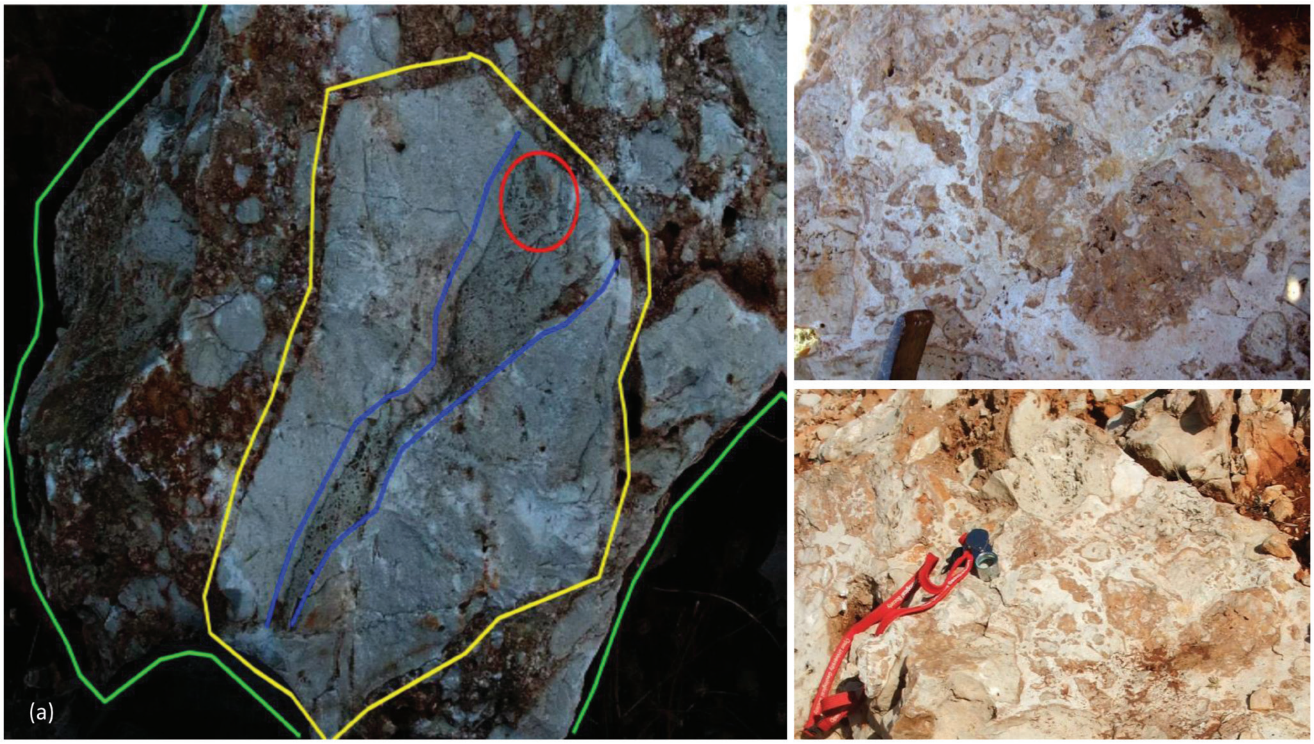

Figure 10: Up to 4 generations of breccia-in-breccia have been observed many times around the study area. In image (a) a monomict clast (red) in a monomict dike (blue) is cutting through a limestone fragment (yellow) itself being a clast of polymict breccia (green).

Figure 11: Breccia-in-breccia.

Figure 12: Fitted fragments occur in micro clasts (c), macro clasts (a, b, d) and mega clasts (e).

Evidence of impact-induced spallation in rocks [12] is seen frequently on the beaches around the study area (Figure 13). Spallation is indicative of a rarefaction wave having passed through a structure, cracking it into slices, while still leaving the rock in its original form. This dynamic shock deformation is also observed on a microscopic scale [2].

Decarbonization/carbonate melt

In contrast to silicate rocks, carbonate rocks do not quench to form glass. Under impact high pressure/temperature (PT) conditions, limestone can melt or decarbonize with subsequent, in part immediate, recrystallization. Like in other impact structures with a partial carbonate target, e.g., Azuara/Rubielos de la Cérida, Spain [13]; Haughton Dome, Canada [14], such relics of carbonate melt/decarbonization are abundant in the investigated area. On Kastellorizo, a white, porous carbonate rock was observed in contact with a scour plane of a polymict breccia interpreted as a variety of pseudotachylite (Figure 14a) [15]. Limestone clasts from the central uplift show a vesicular and skeletal texture as probable relics of decarbonization and/or carbonate melt (Figure 14b). In many outcrops in the study area, white powder and agglomerations also suggest decarbonized limestone/dolostone (Figure 14c, d). Remnants of melting /decarbonization with a flow texture can be seen in Figure 15, along with probable carbonate melt remains of white filaments and plastically deformed limestone components.

Petrographic thin-section analyses

Impact shock deformation in quartz is well documented in contrast to shock effects on carbonate minerals like calcite [16]. However, we observe abundant occurrences of multiple sets of micro-twinning in calcite, frequently in combination with kink banding (Figure 16). Regularly the size of the twins is of the order of 1 μm (Figure 16), which points to high-pressure deformation similar to the development of shock-produced planar deformation features (PDFs) in quartz [16, 17].

Accretionary lapilli and lapillistone, usually associated with volcanic eruptions but also occurring in meteorite impacts, add to geological conspicuousness (Figure 17).

Magnetic susceptibility analyses

A handful of breccias were tested for magnetic susceptibility (Figure 18) using a Bartington MS2 meter with MS2K sensor.

Figure 13: Beach rocks showing spallation.

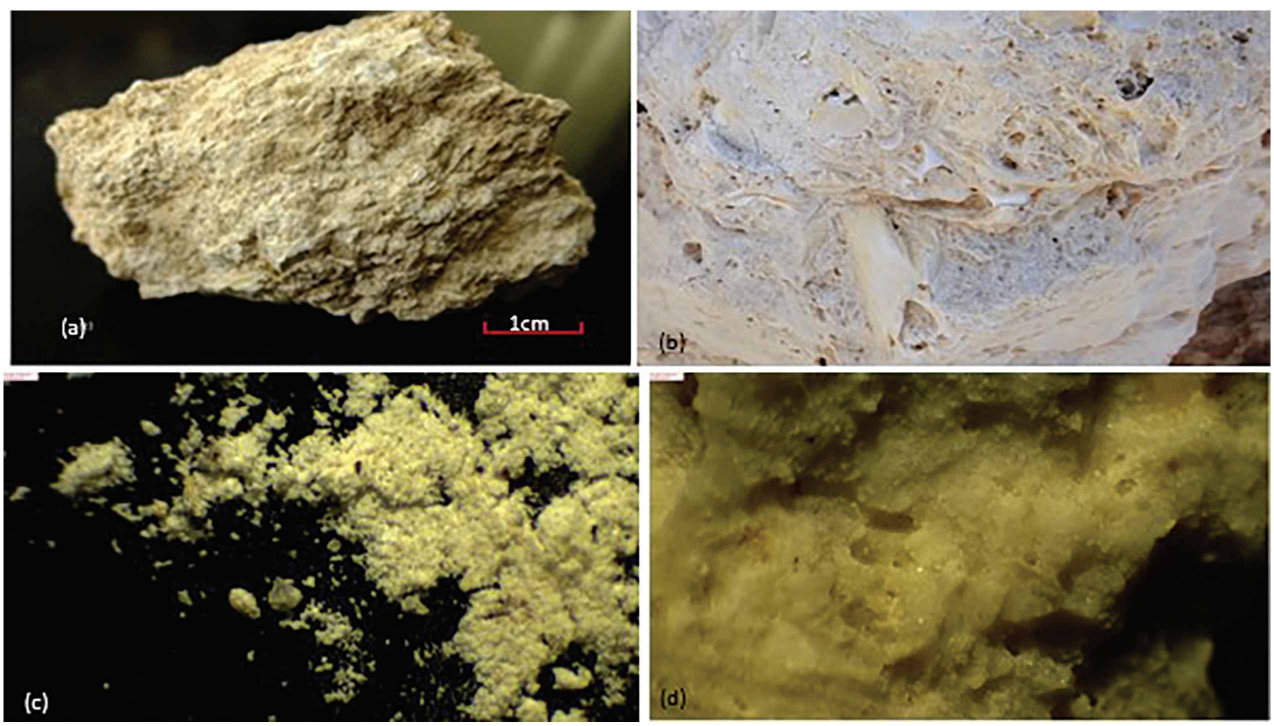

Figure 14: Relics of recrystallized decarbonized limestone/carbonate melt are abundant in the study area. Images a, b, c, and d are described in the text.

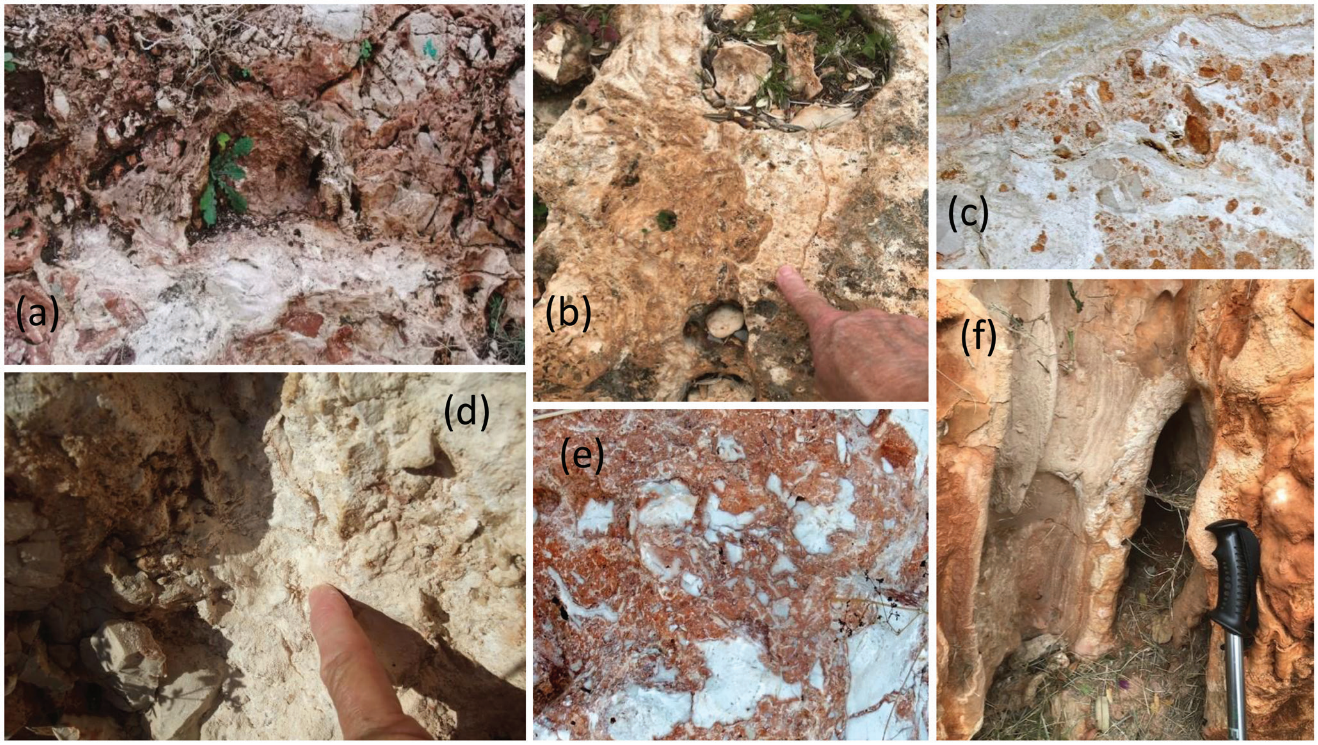

Figure 15: Relics of melting/decarbonization with flow texture a, b, c, d, and f; with plastically deformed limestone components and white filaments, e.

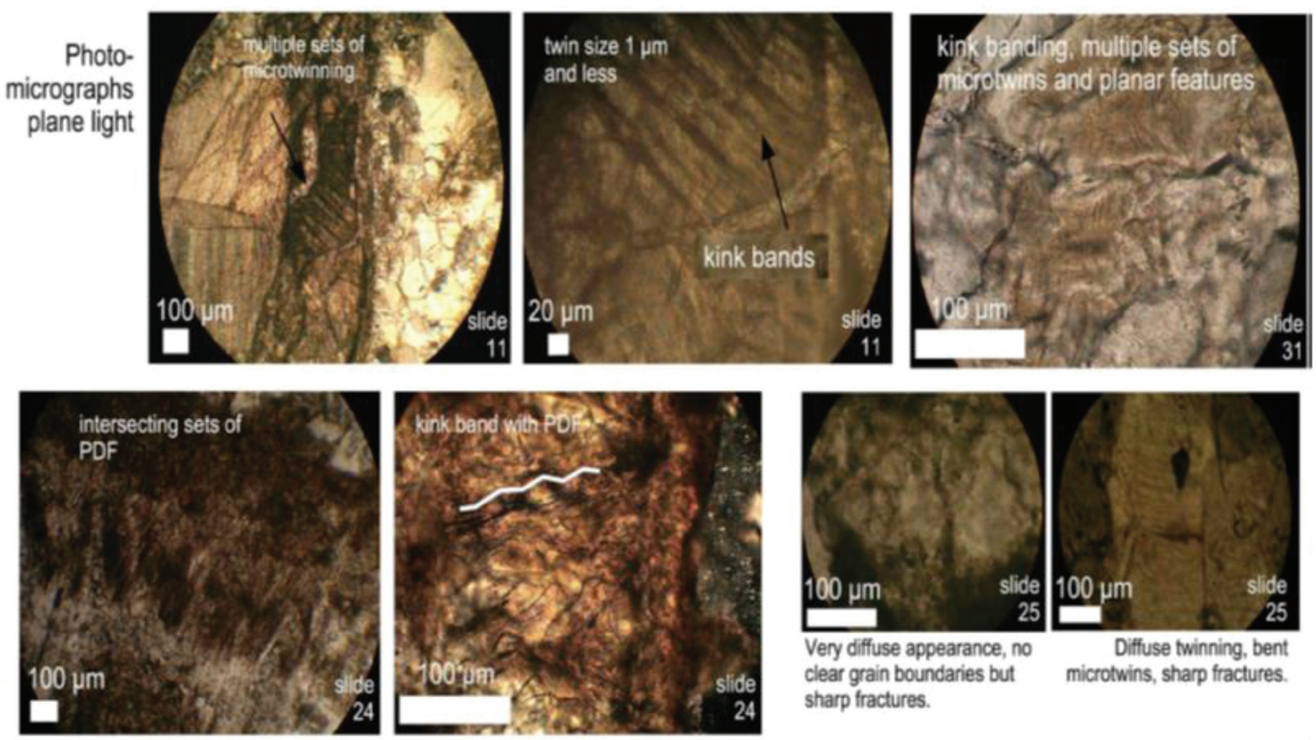

Figure 16: Multiple sets of densely grouped micro-twinning and kink banding in calcite indicating shock metamorphism equivalent to PDFs in quartz.

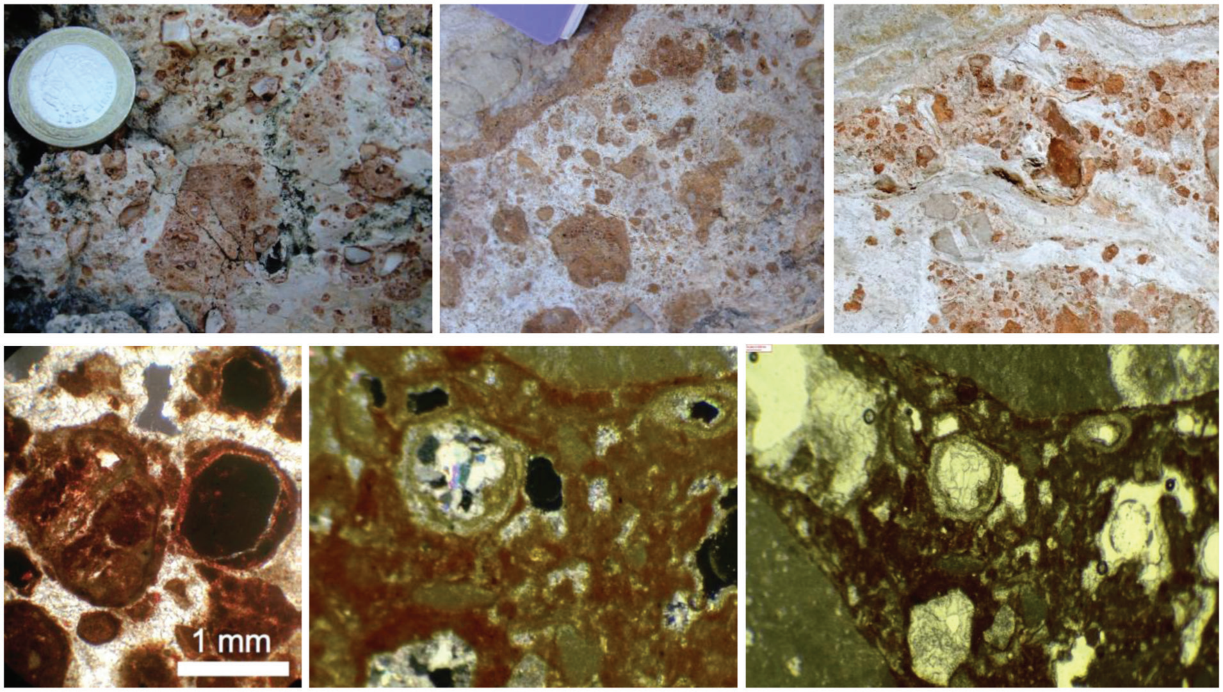

Figure 17: Top row – Lapillistone. Bottom row - accretionary lapilli photomicrographs in both crossed and plane polars.

			Individual MS readings				
Specimen #	Magnetic Susceptibility (x10^{-5} SI)	Brief description	1.0	2.0	3.0	4.0	5.0
RW 11	3.4	Limestone with some matrix in fractures	3.0	3.3	3.4	3.6	3.6
RW 12	108.5	Some limestone in matrix	108.3	108.4	108.5	108.5	108.6
RW 13	3.3	Limestone with some matrix in fractures	3.0	3.2	3.4	3.5	3.5
RW 14	81.9	Some limestone in matrix	81.8	81.9	81.8	81.9	81.9
RW 15	-1.4	Limestone, no matrix	-1.9	-1.6	-1.3	-1.1	-1.1

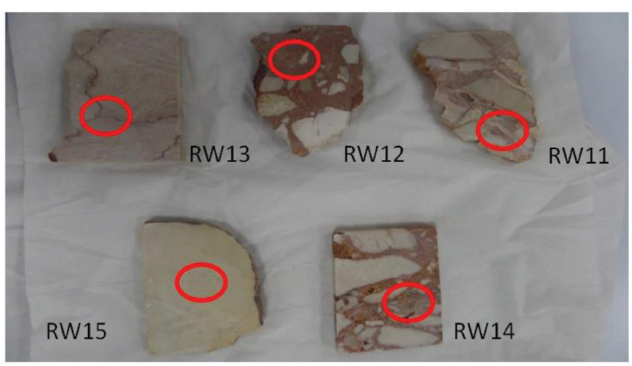

Figure 18: Magnetic Susceptibility results – red ring denotes approximate position of the magnetic susceptibility sensor head.

This revealed relatively strong readings (up to 108×10^{-5} SI) for the carbonate matrix, in comparison to the embedded limestone clasts. Enhanced magnetic susceptibilities in silicate impact breccias are common, but they have also been measured in purely carbonate impactites, though with a more subdued signature [18].

Shatter cones

This accepted indication of an impact structure [1] does not always exist and has not been located in the study area. Shatter cones are usually found around the central uplift, and, as this part of the structure is underwater, any that formed may have suffered dissolution.

Comparison with the Rubielos de la Cérida Structure

The Kaş structure has crystallized in many ways similar to the large Spanish Rubielos de la Cérida impact structure (Figure 19), and the extensive geological impact inventory of Rubielos de la Cérida was a helpful guide in the terrain exploration of the Kaş structure. What is special is that both structures are laid out in a purely sedimentary target, which is also largely formed in carbonate facies.

While the products of meteorite impacts into dense, mostly crystalline and mixed targets are relatively well understood, and macroscopic and microscopic deformation of these target rocks is the norm, the response to an impact into volatile-rich sedimentary rocks, in particular carbonate rocks, remains debated.

Although the impact basin of Rubielos de la Cérida is much more extensive than the Kaş basin and offers more exploration possibilities, it is striking that the morphologies are very similar. This similarity applies to comparable structural conditions, deformation features and rock types right down to the micro range, and it has not been difficult to compare findings of the most varied but impact-typical kind with each other, which is done below (Figures 20-23). Comparable scenarios in the field and in hand-specimen samples are much more extensive but are not presented here in detail. It should first be noted that, in the illustrations, the letters K and R indicate the respective assignment to the two impact structures.

Scour planes are gigantic landslides of mega blocks containing breccias and megabreccias and are typical in larger impact structures. Enormous mass movements often lead to impressive sliding surfaces, partly with mirror polish [19]. They look very similar to tectonic fault

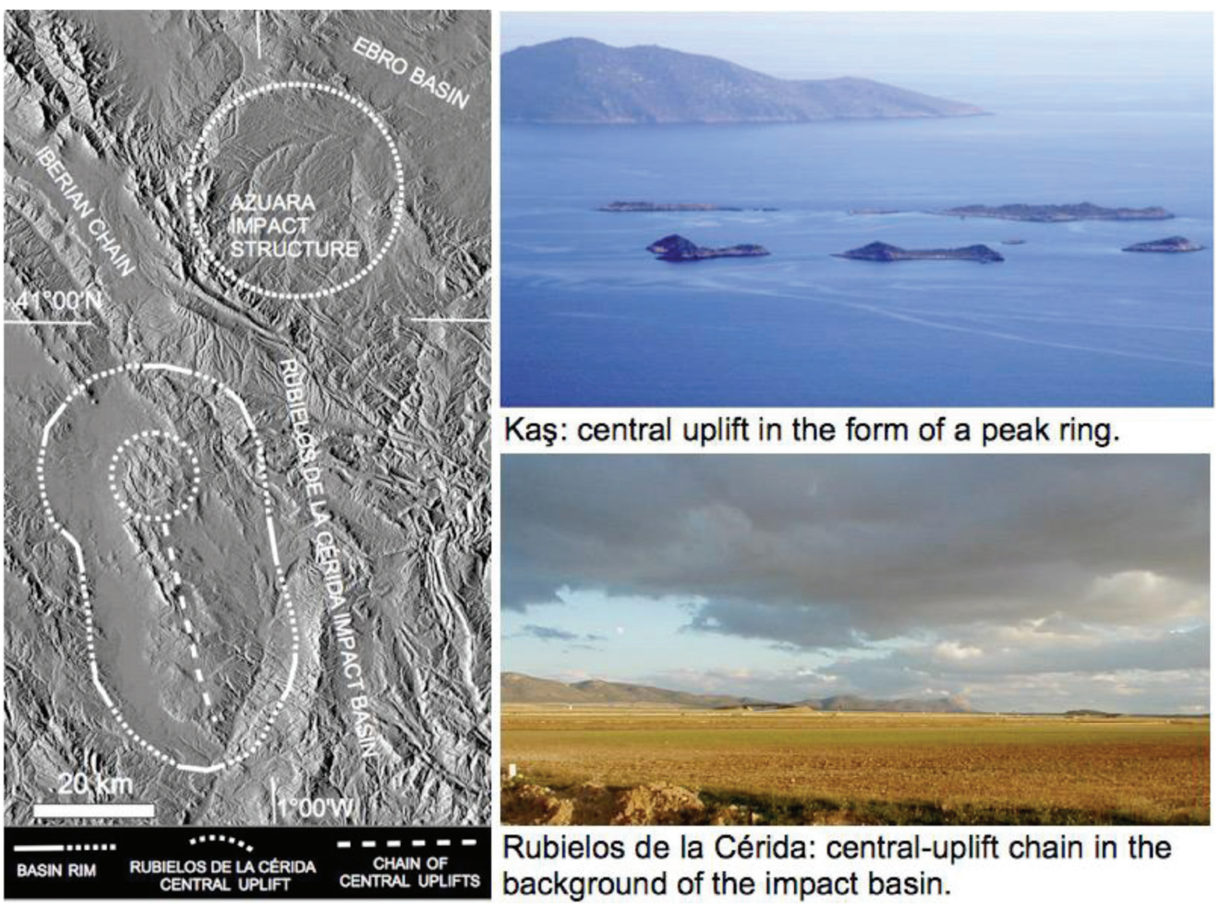

Figure 19: The Azuara and Rubielos de la Cérida impacts in the digital map of Spain 1: 250,000 (courtesy M. Cabedo). Central uplifts (peak ring, Kaş, and chain, Rubielos de la Cérida).

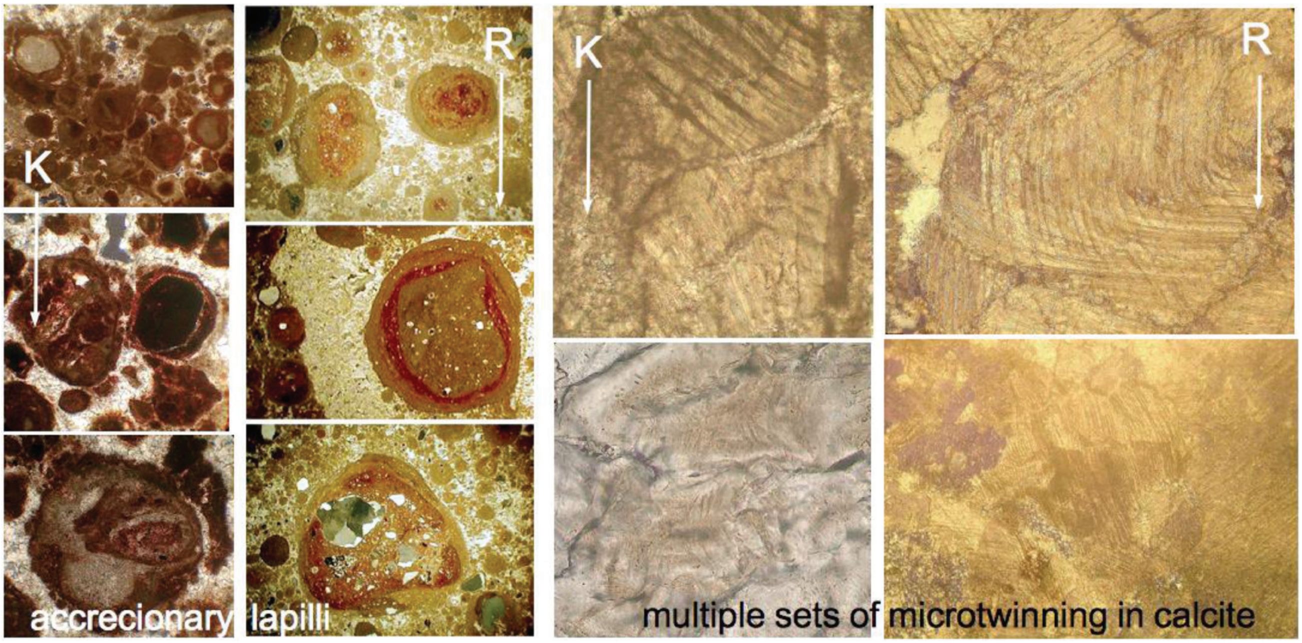

Figure 20: Similarity of photomicrographs under crossed polars of accretionary lapilli (left) and twinning (right) from Kaş (K) and Rubielos de la Cérida (R).

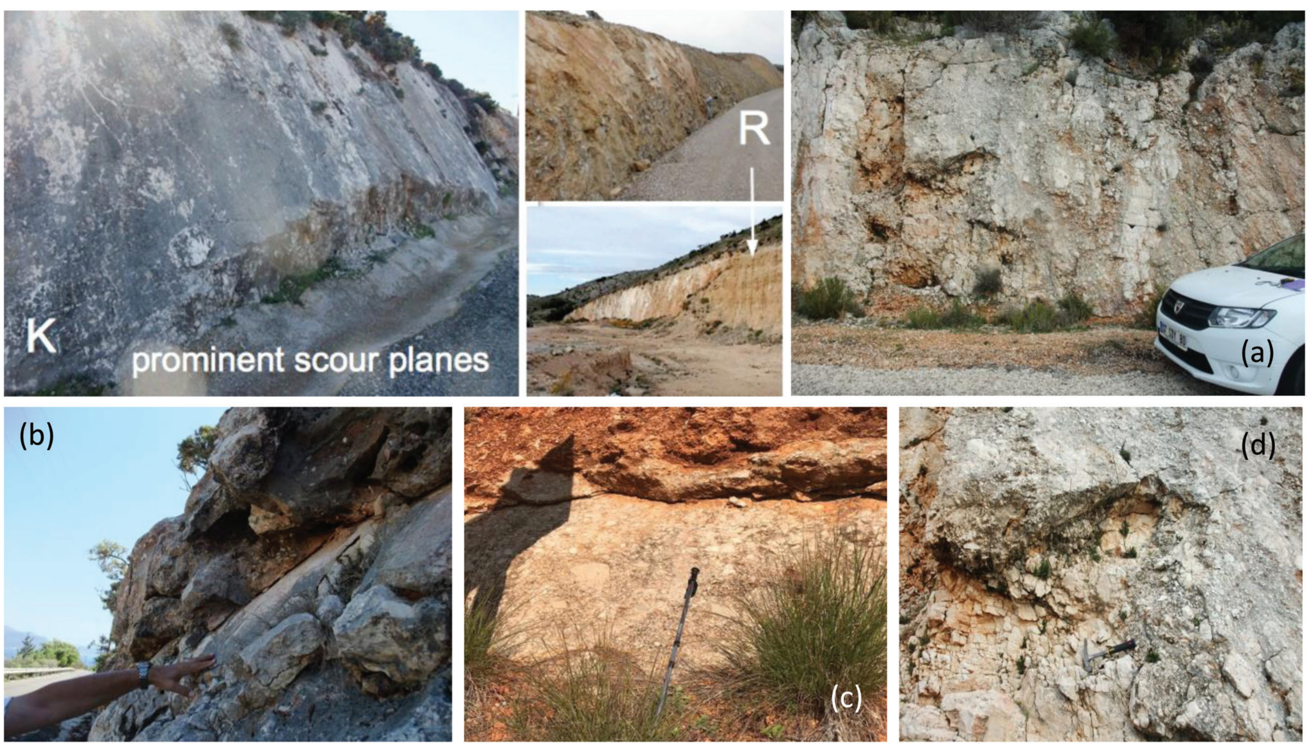

Figure 21: Scour planes showing similarity with Kas (K) and the Rubielos de la Cérida (R). a, b, c and d, indicate the brecciated structure of these features in the Kaş structure.

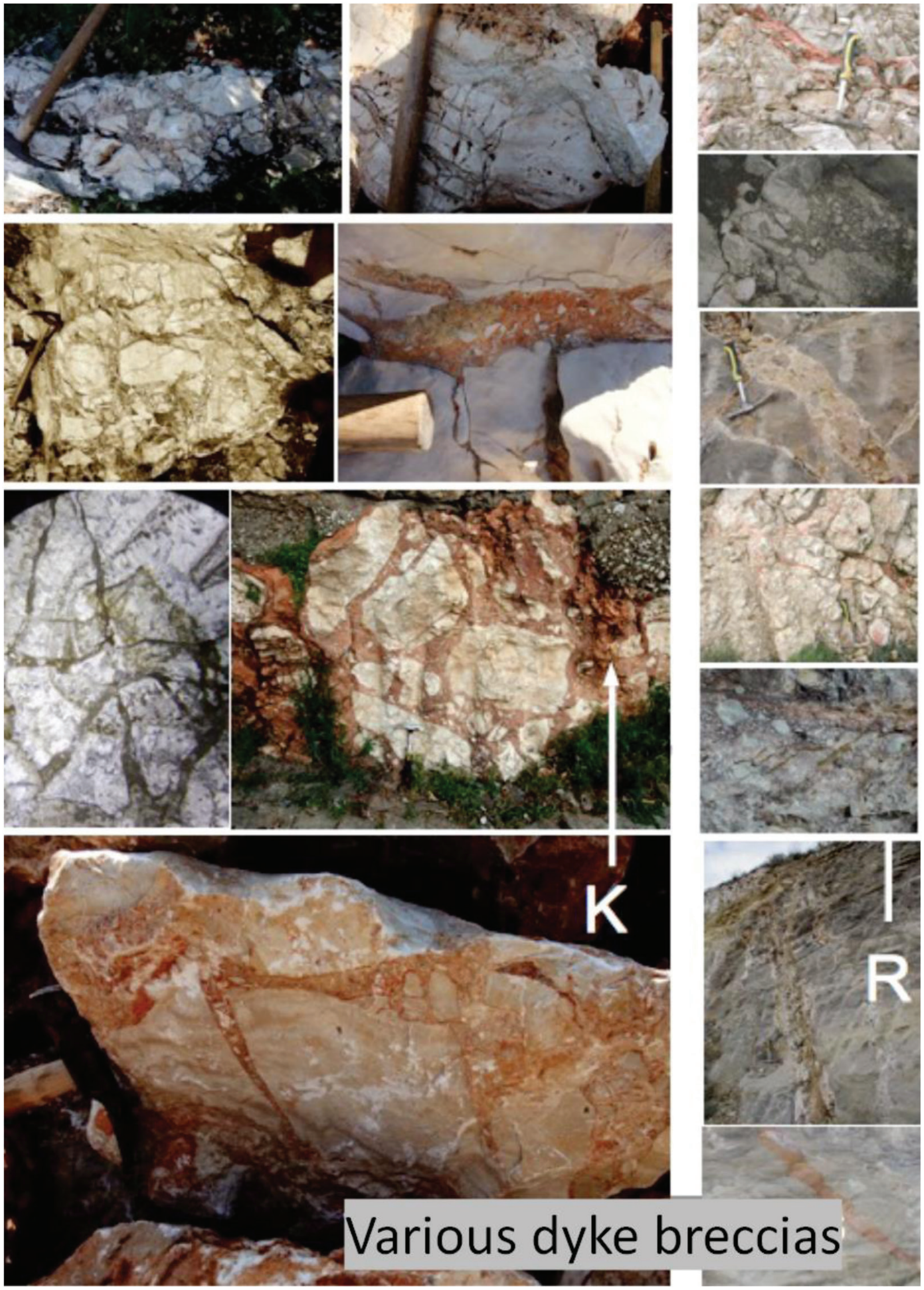

Figure 22: Dyke breccia comparisons between Kaş (K) and the Rubielos de la Cérida (R).

planes, but closer inspection reveals the brecciation within the rock face. Several layers of scour can be observed (Figure 21a-d).

Digital Terrain Modelling

The recently acquired DTM data [9] gave rise to a new area of research, comparing the geology inside the proposed

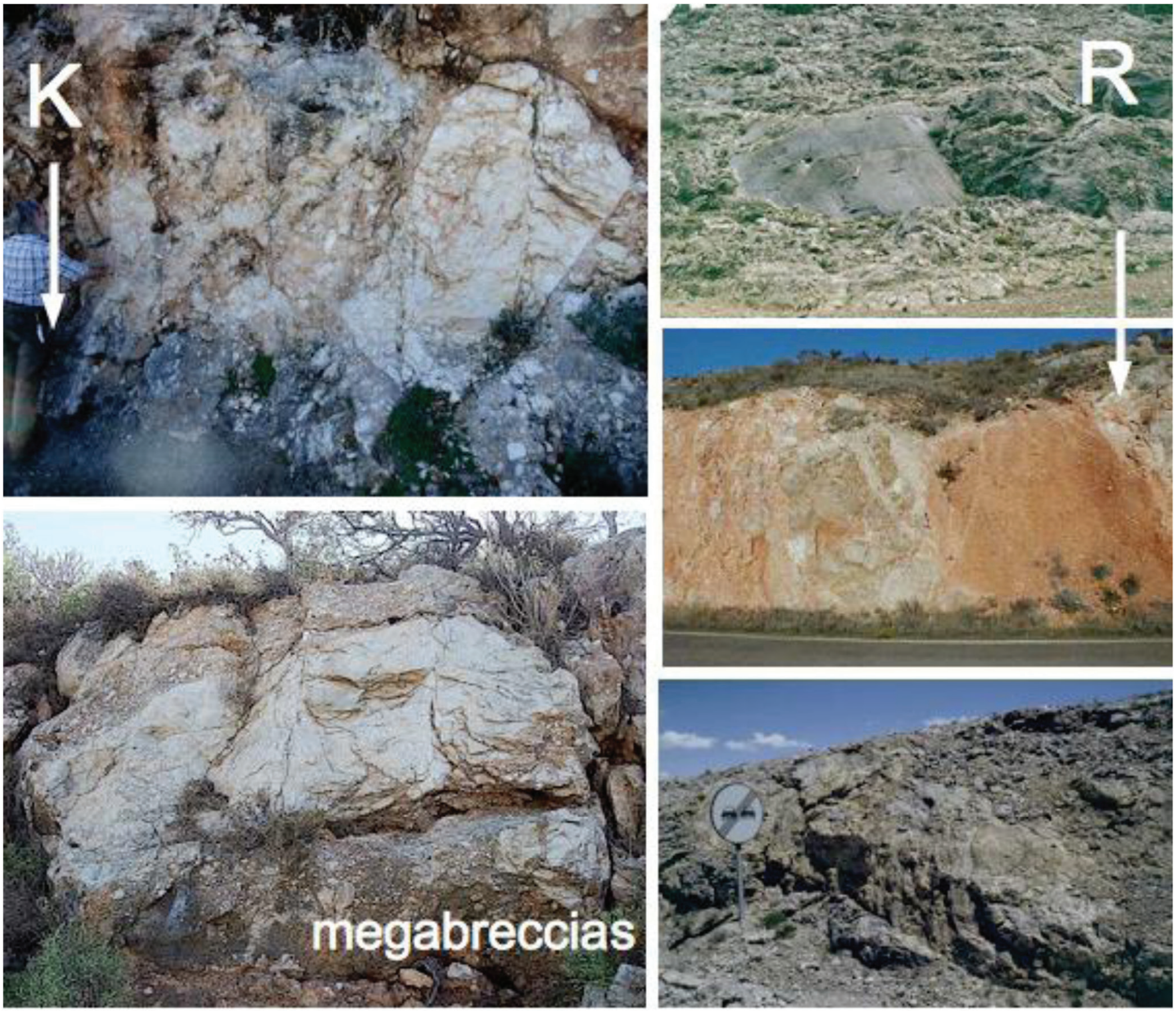

Figure 23: Comparison of megabreccias between Kaş (K) and Rubielos de la Cérida (R).

new suggested crater rim (Figure 4) with that outside. The field results were compelling. Quarries on or inside the proposed rim revealed rocks of generally shattered appearance (Figure 24). Outside the rim, quarrying of large blocks of clean solid limestone was possible to the east of the structure, along with natural tabular limestone (Figure 25a-c), whilst tilting of conglomerates has occurred to the west (Figure 25d-f). None of these latter phenomena were found inside the suggested rim.

A new observation in the limestone inside as opposed to outside the proposed crater was obvious calcite crystals (Figure 26a), observable with the naked eye. The limestone is of a sugary texture (Figure 26b), which indicates that it had been subject to high pressure and temperature, causing the calcite to reorganise into larger crystals, i.e., low- grade metamorphism [20], which can be associated with an impact. This low-grade metamorphism can also explain why the limestone around the water 's edge of Kaş Bay is hard and sharp (Figure 26c) and does not weather the same way outside the study area; limestone in equivalent settings is more rounded and typical of a karstic landscape.

Geomorphology

The topographic view in the southern section of the Teke Peninsula often consists of valleys running parallel to the mountains, which are at varying altitudes and stretch in a northeast-southwest direction; see green lines in Figure 27.

Figure 24: Shattered, brecciated limestone in quarries and main road cuttings on and inside the proposed new crater rim.

Figure 25: a, and b, quarried large blocks of limestone for building stone outside of the proposed crater rim to the east, c, tabular limestone block, d, Conglomerate clast ~1m in length, e, conglomerate blocks, looking south-tilting east, f, conglomerate blocks, looking north-tilting east.

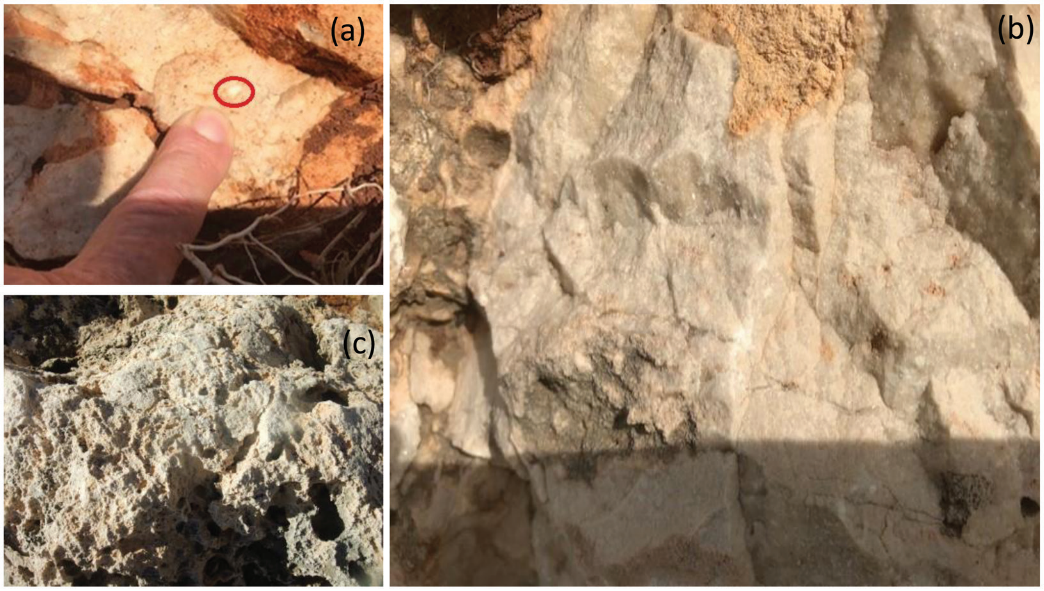

Figure 26: a) enlarged calcite crystal inside red circle, b) sugary textured limestone, c) hard and sharp carbonates.

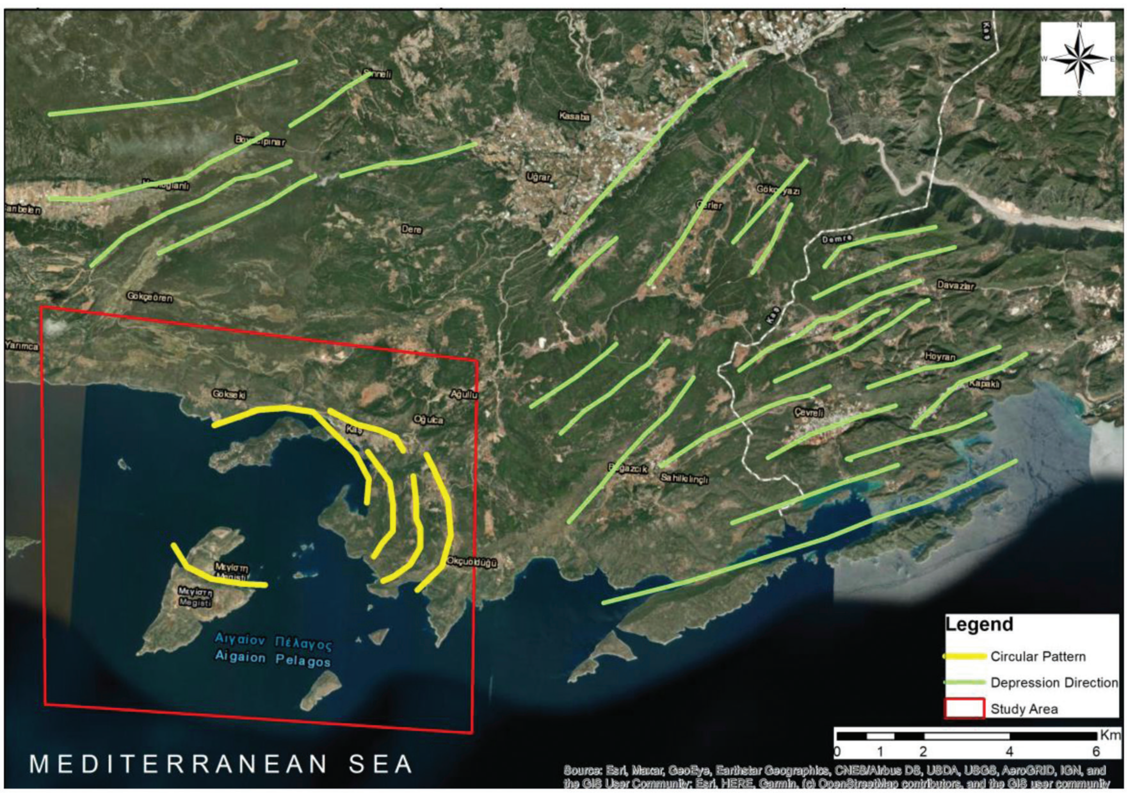

Figure 27: Annotated Google map image, August 2023: Green lines indicate the general northeast-southwest trend in the terrain surrounding the study area in contrast to the yellow lines indicating the concentric geomorphology around Kaş Bay.

On the other hand, terrace-like structures at various altitudes border Kaş Bay in a circular pattern on its immediate eastern side; see yellow lines in Figure 27. These circular terraces, which contrast with the general morphological pattern, are suggested to be marginal collapse zones from the impact cratering modification stage (Figure 28a, b), as

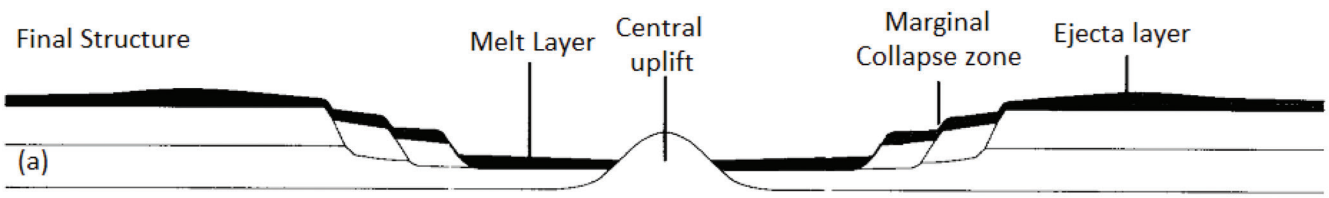

Figure 28a Diagrammatic view of the final structure - 'The development of a complex impact structure' [1].

Figure 28b: Eastern marginal collapse zone of the Kaş Structure looking south. Numbers indicate terraces.

opposed to landslips resulting from general slope instability or from an earthquake. These alternatives would be more linear in their formation.

With the suggested increase in size of the study area from the DTM data, the marginal collapse zone, already clearly observed to the east of the structure (Figure 28b), can now also observed to the north (Figure 29). Although less curved than their eastern counterparts, each terrace to the north conjoins to the corresponding eastern terrace (Figure 28b). This connection of terraces from the north to the east is curved, observable in the foreground of Figure 28b, which implies an impact as the source as opposed to tectonic movement.

The impact is thought to have occurred around 2.5 million years ago, based on stratigraphical evidence, uplift and subsidence in the region [2]. During this time, the shape of the larger suggested study area, indicated in Figure 4, has lost the general concentric configuration expected in an impact structure. This is explained by conflicting tectonic plate movement (Figure 3). Furthermore, with the implied

Figure 29: Marginal collapse zone to the north of the structure showing 3 terraces which correlate to the eastern marginal collapse zone. The turquoise lines correspond to two of the probable transtensional troughs indicated in Fig. 4.

increased size of the structure, the lack of the southern edge is explained not only by the movement of the three aforementioned tectonic plates but also by the proximity of the continental shelf edge (Figure 3). Due to its location, this southern part of the structure will most likely have been less stable than its northern mainland counterpart, and with ~2.5 million years of plate movement and local tectonic activity, this structural instability will have been compromised into collapsing and sliding down the shelf edge as indicated in (Figure 3). Additionally, the prevailing weather is from the southwest adding erosion to the depletion of the structure.

Index - Sample analysis

Sample analysis by pXRF - Niton XL3t 900 and XRF - Rigaku NEX-CG - produced some interesting results, although nothing conclusive. See Tables 1 and 2. These will be further analysed using SEM – EDS.

Discussion/Conclusion

Very large impact structures in purely sedimentary, in particular predominantly carbonate targets, are rare and have not been much investigated to date. Even in recent publications, e.g., in Pilles et al "Review of impact melt and breccia dykes in terrestrial impact structures" [21], sedimentary targets are mentioned only casually in a single sentence about lithic breccia dykes, apparently forgetting that such an inventory exists to a much greater extent and variability as exemplified here. Below is the list of intrinsic geological, geomorphological, petrographic, and mineralogical field evidence found so far on the Kaş Bay impact site. We suggest this testimony should be given considerably more credit by the impact community when ascertaining the provenance of an impact structure, especially an all-carbonate structure such as Kaş Bay. To date 20 types of field evidence have been observed from macro scale to micro, as follows:

Macro:

1) Central uplift.
2) Marginal collapse zones.
3) Impact Breccia – from mega to micro clasts.
4) Polymict and monomict breccia.
5) Breccia in breccia – up to 4 generations.
6) Breccia dykes large and small on land and under water.
7) Fitted fragments.
8) Carbonate melt rocks, some with flow texture.
9) Decarbonized limestone.

Table 1: Initial XRF and pXRF results.

	Mg	Al	Si	S	Cl	K	Ti	Zr	Cr	Fe	Ni	Cu	Zn	Rb	Sr
XRFppm															
69	10600.00	13800.00	21600.00	160.00	128.00	1250.00	996.00	2600.00	26.00	8540.00	18.00	ND	27.00	12.00	45.00
72	4850.00	35000.00	42700.00	153.00	237.00	1760.00	2610.00	3650.00	51.00	22500.00	43.00	ND	53.00	24.00	41.00
73	6070.00	45300.00	57800.00	218.00	183.00	2550.00	3260.00	3750.00	80.00	29900.00	ND	ND	71.00	30.00	40.00
76	2720.00	8630.00	12600.00	289.00	139.00	708.00	688.00	2860.00	22.00	5670.00	18.00	ND	16.00	7.00	73.00
77	1750.00	15300.00	22900.00	335.00	160.00	119.00	118.00	3250.00	25.00	12200.00	ND	ND	37.00	12.00	44.00
80	1970.00	911.00	956.00	170.00	96.00	162.00	81.00	2630.00	ND	167.00	ND	11.00	12.00	ND	241.00
82	2690.00	471.00	378.00	590.00	650.00	93.00	55.00	2470.00	4.00	78.00	ND	10.00	12.00	ND	199.00
84	7090.00	67300.00	87400.00	183.00	228.00	4430.00	5170.00	4270.00	194.00	54600.00	ND	ND	96.00	46.00	63.00
85	1480.00	814.00	677.00	166.00	428.00	108.00	82.00	2650.00	ND	277.00	ND	4.00	7.00	ND	92.00
88	73800.00	512.00	586.00	1160.00	1670.00	145.00	38.00	2210.00	13.00	193.00	ND	10.00	11.00	ND	310.00
94	1390.00	2060.00	1640.00	45.00	71.00	141.00	150.00	2520.00	10.00	1220.00	ND	5.00	10.00	ND	10.00
96	9610.00	12200.00	16600.00	182.00	135.00	781.00	866.00	2930.00	51.00	8310.00	21.00	ND	33.00	6.00	30.00
101	4180.00	13200.00	21800.00	456.00	2200.00	1700.00	1010.00	3360.00	36.00	7470.00	16.00	ND	28.00	11.00	31.00
102	2850.00	500.00	456.00	722.00	702.00	112.00	ND	2920.00	9.00	136.00	ND	15.00	19.00	ND	214.00
pXRF ppm															
70-1	< LOD	57027.19	117155.6	< LOD	< LOD	5820.02	4456.83	141.8	124.49	33002.04	156.83	< LOD	57.13	30.07	71.2
70-2	< LOD	34880	70930.96	< LOD	< LOD	2801.96	1990.84	119.59	62.24	12969.54	248.3	< LOD	19.82	16.02	42.77
98-1	< LOD	23337.15	61080.54	1879.1	2719.52	3690.52	1502.27	59.62	51.58	10624.33	172.04	< LOD	< LOD	17.38	185.23
98-2	26476.57	15190.04	30874.11	3674.41	1740.53	2059.99	1156.76	45.5	40.83	6881.87	109.46	< LOD	< LOD	13.97	134.54
98-3	< LOD	17468.63	46505.46	27061.71	2741.96	3188.25	1394.7	53.14	49.49	9831.03	162.18	< LOD	23.6	19.4	128.4
100-1	< LOD	16066.57	39084.72	461.13	5792.38	3670.06	1465.78	43.6	59.38	9100.79	121.05	< LOD	22.06	16.03	62.34
100-2	< LOD	7373.58	14711.19	1236.17	2205.55	1404.27	747.34	22.21	< LOD	2003.64	281.85	< LOD	< LOD	8.3	44.77
100-3	< LOD	11080.71	30753.76	254.56	30139.09	2941.88	1084.14	44.15	52.74	7129.06	103.92	< LOD	< LOD	15.82	43.86
74-1	< LOD	25002.88	45865.05	< LOD	< LOD	2381.65	1962.93	46.48	81.46	11708.53	177.58	< LOD	24.47	10.41	13.73
74-2	< LOD	38486.28	58992.88	< LOD	< LOD	2649.98	2007.64	59.53	78.48	13195.25	275.41	< LOD	28.34	9.8	17.92
74-3	< LOD	30927.37	54448.42	< LOD	< LOD	2695	1936.26	51.33	52.22	10176.97	228.63	< LOD	35.8	10.19	17.34
74-4	< LOD	42104.42	75765.19	217.5	< LOD	3087.72	3227.93	56.18	< LOD	16213.75	< LOD	< LOD	29.4	10.27	15.39
74-5	< LOD	21938.38	41188.92	< LOD	< LOD	1486.75	1658.79	65.87	60.33	9860.56	246.74	< LOD	< LOD	6.83	15.07
71-1	< LOD	30266.56	50836.77	1067.66	114.01	3438.24	1765.78	74.29	65.45	11754.7	199.84	< LOD	< LOD	11.97	20.1
71-2	< LOD	34082.46	59416.11	< LOD	< LOD	4383.84	2012.61	86.72	59.95	14344.48	207.96	< LOD	< LOD	19.18	27.89
71-3	< LOD	55410.29	83488.48	< LOD	< LOD	5923.84	3190.61	70.5	98.2	21496.53	275.2	< LOD	35.72	16.23	28.61
97-1	< LOD	10222.64	19683.76	328.82	< LOD	674.64	813.73	22.57	< LOD	2584.08	272.1	< LOD	< LOD	< LOD	55.85
97-2	< LOD	19398.5	40075.62	243.49	123.67	2324.37	1814.81	24.34	50.54	6448.21	108.39	< LOD	44.47	< LOD	22.27
85b-1	< LOD	< LOD	6189.35	877.71	37869.91	415.86	696.76	< LOD	< LOD	692.27	217.65	< LOD	< LOD	< LOD	39.4
85b-2	< LOD	7115.88	3037.84	2438.32	41499.86	< LOD	< LOD	< LOD	< LOD	370.35	577.52	< LOD	< LOD	< LOD	133.75
85b-3	< LOD	< LOD	2526.72	738.32	16125.51	< LOD	< LOD	< LOD	< LOD	1855.6	205.47	< LOD	< LOD	< LOD	17.69
89	47506.98	< LOD	4555.96	197.92	417.23	< LOD	< LOD	< LOD	< LOD	198.69	< LOD	< LOD	< LOD	< LOD	145.83
78-1	< LOD	21472.31	41488.76	< LOD	< LOD	3375.23	1085.03	79.43	< LOD	11223.9	281.21	< LOD	39.97	14.26	37.84
78-2	< LOD	20466.93	40336.02	< LOD	< LOD	2388.32	1297.16	81.57	115.75	12015.59	145.83	< LOD	34.24	12.26	42.63
78-3	< LOD	19509.17	36666.76	< LOD	< LOD	2008.54	1580.84	56.67	51.36	11819	286.98	< LOD	< LOD	14.34	39.2
78-4	< LOD	11988.76	24954.85	< LOD	< LOD	1083.3	646.08	76.93	< LOD	7433.44	516.3	< LOD	38.32	13.57	27.61
95-1	< LOD	56498.64	104402.09	140.63	< LOD	6486.88	4811.82	128.92	130.28	26996.53	218.22	45.55	74.73	33.37	41.67
95-2	< LOD	59581.9	105402.28	441.72	< LOD	5592	3458.93	127.64	80.33	22040.38	298.7	< LOD	76.13	31.79	41.35
95-3	< LOD	55927.81	100117.4	< LOD	< LOD	5059.09	3338.74	128.7	108.52	25311.62	252.54	38.68	52.39	36.33	44.91
78b	< LOD	19110.58	40325.3	163.85	< LOD	1729.18	1102.88	55.06	32.17	6082.91	405.41	< LOD	25.59	4.97	34.33

Table 1: Continued

	Mg	Al	Si	S	Cl	K	Ti	Zr	Cr	Fe	Ni	Cu	Zn	Rb	Sr
78b2	< LOD	28526.65	51288.92	139.82	< LOD	3215.13	1523.29	55.25	71.07	11590.02	190.37	< LOD	31.1	11.26	32.97
78b3	< LOD	22793.32	61755.41	1464.23	114.89	2688.64	1184.09	45.72	80.85	5888.55	187.69	< LOD	85.02	7.07	48.3
78b4	< LOD	29321.06	56447.82	256.83	< LOD	3021.68	1730.47	72.15	45.8	13429.7	142.31	< LOD	39.53	12.47	49.4
92	< LOD	29783.8	48185.51	< LOD	< LOD	2995.61	1432.26	30.33	72.43	10147.57	231.91	< LOD	< LOD	7.15	64.32
92-2	< LOD	< LOD	5833.62	< LOD	< LOD	< LOD	< LOD	< LOD	< LOD	629.21	344.32	< LOD	< LOD	< LOD	7.59
92-3	< LOD	24080.79	33857.99	< LOD	707.75	2707.1	1303.13	54.53	65.44	13468.26	459.36	60.68	42.93	16.19	30.3
92-4	< LOD	< LOD	3486.64	< LOD	< LOD	< LOD	< LOD	< LOD	55.01	494.75	202.93	< LOD	< LOD	< LOD	259.37
87-1	< LOD	5206.93	18370.67	2196.68	7662.33	937.12	< LOD	< LOD	< LOD	1200.84	< LOD	< LOD	< LOD	< LOD	998.32
87-2	< LOD	4747.26	9735.93	5035.6	5133.4	1024.84	< LOD	< LOD	< LOD	463.44	270.63	< LOD	< LOD	< LOD	7313.26
87-3	38632.37	< LOD	8679.29	5025.84	17616.91	932.27	< LOD	< LOD	< LOD	530.84	< LOD	< LOD	< LOD	< LOD	2421.65

< LOD – less than limit of detection. Highlighted figures were shown in parentheses on the original data sheet. ND – No data.

Table 2: XRF results showing REE along with Au and Ir.

	Au	Sn	Y	Br	Th	Tm	Ta	Ir	Te	Pa	Eu	Re	Tb	Dy	Er
XRFppm															
69	ND	30.00	8.00	11.00	ND	30.00	13.00	ND	ND	10.0000	1080.00	14.0000	253.00	ND	67.00
72	ND	31.00	43.00	5.00	14.00	50.00	13.00	ND	13.000	14.0000	20000.00	21.0000	594.00	ND	73.00
73	ND	33.00	33.00	7.00	16.00	56.00	ND	17.000	ND	19.0000	2980.00	15.0000	736.00	ND	67.00
76	ND	28.00	6.00	7.00	ND	15.00	ND	ND	12.000	9.0000	1040.00	26.0000	280.00	54.00	113.00
77	ND	36.00	10.00	13.00	ND	ND	11.00	ND	18.000	17.0000	2000.00	16.0000	552.00	ND	109.00
80	ND	27.00	ND	ND	ND	ND	16.00	ND	ND	ND	622.00	15.0000	127.00	45.00	ND
82	ND	23.00	ND	5.00	ND	ND	14.00	ND	ND	ND	130.00	11.0000	43.00	29.00	ND
84	12.000	47.00	49.00	6.00	25.00	ND	37.00	21.000	26.000	25.0000	4150.00	25.0000	1340.00	178.00	72.00
85	ND	25.00	ND	3.00	ND	ND	ND	ND	ND	ND	ND	6.0000	58.00	ND	ND
88	ND	22.00	ND	8.00	ND	ND	ND	ND	ND	2.0000	ND	4.0000	32.00	18.00	12.00
94	ND	21.00	ND	ND	ND	ND	ND	ND	12.000	ND	ND	ND	ND	ND	18.00
96	ND	30.00	6.00	19.00	9.00	40.00	19.00	ND	ND	9.0000	1230.00	24.0000	311.00	61.00	77.00
101	ND	33.00	7.00	31.00	10.00	ND	ND	ND	ND	11.0000	2120.00	22.0000	492.00	ND	102.00
102	11.000	31.00	ND	6.00	ND	ND	ND	ND	11.000	ND	ND	13.0000	84.00	68.00	ND

Highlighted figures were shown in parentheses on the original data sheet. ND – No data.

10) Spallation.
11) Scour planes.
12) Sugary limestone containing visible calcite crystals.
13) Possible transtension troughs and transpression ridges on land and underwater.
14) Lapillistone.

Micro:
15) Fitted fragments.
16) Spallation.
17) Accretionary lapilli.
18) Multiple sets of calcite micro-twining often with kink bands.
19) Regularly; Size of micro-twining to the order of 1 μm, similar development to PDFs in quartz.

Electromagnetism:
20) Increased magnetic susceptibility.

The DTM data indicating a larger structure is supported by the newly observed field evidence, making the Kaş Bay Impact Structure much larger than originally suspected, with a diameter in the region of 20 km. The alteration in the expected concentric geomorphology of an impact structure is explained by the movements of three tectonic plates over time.

Sample analysis by pXRF, XRF, petrology and magnetic susceptibility has produced some interesting data and is ongoing, with results to be provided in a future publication.

The abundance of field evidence and related geomorphology makes it increasingly difficult to envisage a cause other than an impact for the features of this study area. We, therefore, propose that the Kaş Bay Impact Structure be added to the list of known terrestrial impact structures.

Acknowledgements

We wish to thank the Open University Ian Gass bursary committee and the Geologists' Association for supporting this project along with the following for their help in both the field and laboratories: Eleanor Ross, and Ian Chaplin from Durham University, Özge Özer from Akdeniz University, Dr Bariş Semiz from Pamukkale University, Ozan Ünsalan from Ege University, from Turkey - Belma Namlı, Saygin Özatmacca, from Greece -Pantazis Houlis, Manolis Roxanus, from England - Mike Stockbridge, Paul Forrester, Dave Talbot, Kenneth Harvey, Alex and Emma Hilton.

References

[1] French, B.M. *Traces of Catastrophe: A Handbook of Shock Metamorphic Effects in Terrestrial Meteorite Impact Structures*; LPI: Houston, 1998; pp 120.

[2] Ure, A.; Westaway, R.; Bridgland, D.R.; Demir, T.; Ernstson, K. Abstract #1455: Impact Hypothesis for the Kaş Bay Structure (Turkey/Greece) Strengthened. In *LPSC XLIX*, 2018.

[3] Ernstson, K.; Claudin, F. Abstract #1827: Transpression and Transtension Impact Cratering Features: The Steinheim, Saarlouis (Both Germany) and Singra-Jiloca (Spain) Cases. In *LPSC LIII*, 2022.

[4] Huang, Z. S. *Speed of the Continental Plates.* The Physics Factbook. 1997. Available online: https://hypertextbook.com/facts/1997/ZhenHuang.shtml. (accessed July 2023).

[5] Konak, N.; Şenel, M. 1/500000 Scaled Geology Map of Turkey, Denizli Sheet. General Directorate of Mineral Research and Exploration: Ankara, Turkey, 2002.

[6] French, B.M.; Koeberl, C. The Convincing Identification of Terrestrial Meteorite Impact Structures: What Works, What Doesn't, and Why. *Earth-Sci. Rev.* **2010**, *98*, 123–170; doi: 10.1016/j.earscirev.2009.10.009.

[7] Ure, A.; Westaway, R.; Bridgland, D.R.; Ernstson, K. Abstract #1144: Evidence for a Meteorite Impact Structure on the Turkey-Greece Frontier. In *LPSC XLVIII*, 2017.

[8] Open Water Swimming Association. *Meis – Kaş, Greece-to-Turkey Cross-Border Swim*. 2019. Available online: https://www.openwaterswimming.com/meis-kas-greece-to-turkey-cross-border-swim/ (accessed July 2023).

[9] Available online: www.mapzen.com/blog/terrain-tile-service/ (accessed December 2022).

[10] Lambert, P. *Breccia Dikes: Geological Constraints on the Formation of Complex Craters*. In *Multi-Ring Basins: Formation and Evolution, Proc. Lunar Planet. Sci. 12A*, Merrill, R.B., Schultz, P.H., Eds.; 1981, pp. 59–78.

[11] Ernstson, K.; Claudin, F. Impact Breccia Generations Crooked Creek. Available online: http://www.impact-structures.com/?s=breccia+in+breccia (accessed on 10 September 2023).

[12] Ernstson, K. Meteorite Impact Spallation from Mega- to Micro-Scale. 2014. Available online: https://www.academia.edu/29849538/impact-educational/meteorite-impact-spallation-from-mega-to-micro-scale.

[13] Ernstson, K.; Claudin, F.; Schuessler, U.; Hradil, K. The Mid-Tertiary Azuara and Rubielos de la Cérida Paired Impact Structures (Spain). Treballs del Museu de Geologia de Barcelona, **2002**, 11, 5–65; doi: 10.1071/ASEG2004ab026.

[14] Osinski, G.R.; Lee, P.; Spray, J.G.; Parnell, J.; Lim, D.S.S.; Bunch, T.E.; Cockell, C.S.; Glass, B. Geological overview and cratering model for the Haughton impact structure, Devon Island, Canadian High Arctic. *Meteorit. Planet. Sci.* **2005**, *40*, 1759–1776; doi: 10.1111/j.1945-5100.2005.tb00145.x.

[15] Reimold, W.U. Pseudotachylite in Impact Structures — Generation by Friction Melting and Shock Brecciation? A Review and Discussion. *Earth-Sci. Rev.* **1995**, 39, 3–4, 247–265;doi: 10.1016/0012-8252(95)00033-X.

[16] Bell, M.S. Abstract #1321: Relative Shock Effects in Mixed Powders of Calcite, Gypsum, and Quartz: A Calibration Scheme from Shock Experiments. In *LPSC, XL*, 2009.

[17] Short, N.M.; Gold, D.P. *The Manson Impact Structure, Lowa; Anatomy of an Impact Crater;* Geological Society of Amer. Special Paper, 1996; 302, pp 245–266.

[18] Duncan, C.; Gordon C. Enhancement of Magnetic Signatures of Impact Structures. ASEG Extended Abstracts, **2004**, *1*, 1–4, doi: 10.1071/ ASEG2004ab02.

[19] Ure, A.; Westaway, R.; Bridgland, D.R.; Claudin, F.; Ernstson, K. Abstract #1196: Kaş (Turkey/Greece) and Rubielos de la Cérida (Spain) Meteorite Impact Structures: Comparative Insights into Prominent Sedimentary Carbonate Targets. In *LPSC*, 2019.

[20] Rhea, M. Limestone: Identification, Pictures and Info for Rock Hounds/Crystalline Limestone. 2023. Available online: http://rockhoundresource.com/limestone (accessed on 21 August 2023).

[21] Pilles, E.A.; Osinksi, G.R.; Grieve, R.A.F.; Tornabene, L.L. Abstract #1994: A Review of Impact Melt and Breccia Dykes in Terrestrial Impact Structures. In *LPSC XLIX*, 2018.